Unraveling the Core of Fuel Cell Performance: Engineering the Ionomer/Catalyst Interface

Chenzhao Li[1,2], Kang Yu[3,4], Ashley Bird[5,6], Fei Guo[7], Jan Ilavsky[8], Yadong Liu[1], David A. Cullen[9], Ahmet Kusoglu [5], Adam Z. Weber[5], Paulo Ferreira[3,4,10]*, and Jian Xie[1]*

[1] Department of Mechanical and Energy Engineering, Purdue School of Engineering and Technology, Indiana University-Purdue University, Indianapolis, Indiana 46202, USA. Email: jianxie@iupui.edu;

[2] School of Mechanical Engineering, Purdue University, West Lafayette, Indiana 47906, USA

[3] Materials Science and Engineering, University of Texas at Austin, Austin, TX, 78712, USA

[4] International Iberian Nanotechnology Laboratory, Braga, Portugal. Email: paulo.ferreira@inl.int

[5] Energy Conversion Group, Energy Technologies Area, Lawrence Berkeley National Laboratory, Berkeley, California 94720, United States

[6] Department of Chemical and Biomolecular Engineering, University of California Berkeley, Berkeley, California 94720, United States

[7] Department of Molecular and Cellular Biology, University of California, Davis, Davis, CA 95616-8665, USA

[8] X-Ray Science Division, Argonne National Laboratory, Lemont, Illinois 60439, USA

[9] Center for Nanophase Materials Sciences, Oak Ridge National Laboratory, Oak Ridge, TN 37831, USA. Email: cullenda@ornl.gov

[10] Mechanical Engineering Department and IDMEC, Instituto Superior Técnico, University of Lisbon, Av. Rovisco Pais, 1049-001 Lisboa, Portugal

1. Experiment detail

Catalyst functionalization and synthesis. The introduction of the NH_2 groups on carbon surface was realized using the diazonium reaction. *P*-phenylenediamine, Vulcan XC72 and nitric acid were mixed in a flask, sonicating using sonication bath, and then the mixture was heated to 65 ℃ in oil bath, and finally sodium nitrite solution was added into the mixture dropwise followed by 18 hrs-heating in an oil bath at 65 ℃. The same method was applied for SO_3H functionalization but replacing *P*-phenylenediamine with sulfanilic acid. After the reaction, the mixture was washed using DI-water and ethanol, then filtered, and dried in a vacuum oven over night at 60 ℃. The synthesized functionalized carbons were analyzed using XPS. The XPS results show the existence of NH_2 and SO_3H groups introduced on carbon surface with covalent bonded (FigS.2). After confirming the covalently bonded NH_2 and SO_3H groups onto carbon surface, then Pt nanoparticles were loaded by reducing precursor (H_2PtCl_2) in mixture of ethylene glycol and DI water at 140 °C for 6 hours. Finally, the dispersion was filtered followed by drying overnight in a vacuum oven at 60 °C over night.

USAXS measurement. The X-ray scattering measurements were conducted at beamline 9ID-C at the Advanced Photon Source (APS), Argonne National Laboratory. The samples of inks after sonication were collected into a glass capillary tube (5 mm diameter, NMR testing tube) and sealed with a rubber cap. The sample tubes were mounted in the beamline hutch and exposed to a 21 keV monochromatic X-ray beam. The scattered intensity was collected within a scattering vector range of 10^{-4} to 1 $Å^{-1}$ by using a Bonse-Hart camera setup for USAXS and a Pilatus 100 K detector for pinhole SAXS. The background scattering data from the capillary tube filled with the corresponding solvent (n-PA/H_2O) was recorded and subtracted from scattering data for each corresponding catalyst ink. The scattering data were analyzed in a modeling macro package Irena for data fitting and simulation on Igor Pro (WaveMetrics, OR) platform.

Cryo-TEM analysis. A 3.0 uL aliquot of the sample was placed on a glow discharged QUANTIFOIL® R1.2/1.3 300 mesh copper grid. It was then plunge-frozen using FEI Vitrobot Mark III with 8 sec blotting at 20 °C. The frozen grid was loaded into 200 kV Thermo Scientific Glacios™ Cryo Transmission Electron Microscope. Low dose images were recorded using Gatan K3 direct electron detector at ×45,000 nominal magnifications (0.88 Å/pixel) with total dose of 45 e/$Å^2$.

SEM Analysis of catalyst layer (MEA CL pore structure). MEAs of pristine-carbon black, NH_2-XC72 and SO_3H-XC72 samples were initially coated with a Gatan-J1 epoxy mixture to improve stiffness, placed in a mold filled with an Araldite® 6005, benzyl dimethylamine and docenyl succinic anhydride mixture, out-gassed to remove air at the MEA/epoxy interface, and cured in an oven at 60 °C for 8 hours. The cured molds were microtomed at room temperature and the electron transparent MEA cross-sections less than 70 nm thick were obtained for TEM observation. To acquire the pore morphology in the MEA CL of three catalysts, a focused ion beam (FIB) coupled with scanning electron microscope (SEM) was utilized in a slice and view mode (Fig.S14). The thickness of each slice was controlled at 10nm, while the current of ion beam was controlled at 7.7pA to mitigate ion beam damage. In addition, the accelerating voltage of electron beam is controlled at 5kV for imaging, after each slicing by the ion beam. A global segmentation was first performed, followed by a manual segmentation and 3D reconstruction to achieve a more precise outline of pores in each image.

TEM analysis of ionomer/catalyst interface

The cathode was scrapped lightly with a razor and the resulting powder was ground and dispersed onto a lacey-carbon film supported on a 200 meshes copper grid. The grids were loaded into a Thermo Scientific Krios G4 cryo-TEM at room temperature, after which the instrument was cooled to cryogenic temperatures. Low-dose, high resolution images were acquired using a Thermo Scientific Falcon 4i direct electron detector with an accelerating voltage set to 300kV.

ITC Measurement

Binding experiments were conducted using a NanoITC (TA Instruments) as previously described[1]. Briefly, ionomer samples are dialyzed in deionized water and then diluted to 3.25 mg/mL for binding to SO_3H-XC72 and XC72 and diluted to 2.75 mg/mL for binding to NH_2-XC72 due to the stronger affinity. Ionomer is titrated into a cell containing 0.5 mg/mL nanoparticle in deionized water. For each experiment, an initial 4 uL ionomer aliquot is injected to remove bubbles; this injection is excluded from the data analysis. Twelve 8 uL aliquots of ionomer were injected into the cell at 25^{o}C, with 900 seconds between the start of each injection. Backgrounds were collected (water into nanoparticle, ionomer into water, and water into water) to subtract heats of dilution/mixing from the results. Each injection peak is then integrated, and the heats are fit to an independent binding isotherm using the NanoAnalyze software (TA Instruments). The association

constant is extracted from the model fit, and error bars are obtained from the confidence interval of the fit.

Surface energy measurement

The surface energy of three carbons with water was measured using the dynamic vapor sorption (DVS) analysis (Micrometrics, Georgia, US). A sample was held at each temperature to reach equilibrium while the mass change of the sample was measured at each temperature (RH). The mass change at each temperature (RH) step was recorded to generate a water vapor sorption (WVS) curve. The water spreading pressure, liquid-solid adhesion work and the surface energy can be extrapolated from the WVS curves[2, 3].

RDE test

All electrochemical measurements were performed using a Biological VSP potentiostat equipped with high-speed rotators (MSR-RDE-E5) from Pine Instruments (Pine Research Instrumentation, Durham, NC). A rotating disk electrode (RDE) from Pine Research Instrumentation was used as the working electrode with a glassy carbon disk: OD = 5.61 mm. A standard hydrogen reference electrode (S.H.E) ET070 (eDAQ Inc, Springs, CO) and a platinum spring counter electrode (99.99%, AFCTR5, Pine Research Instrumentation, Durham, NC) was used in a three-electrode electrochemical cell. To prepare the working electrode, 5 mg catalyst was dispersed ultrasonically in a 5 mL mixture of isopropanol and DI-water to form an ink. The ink was then drop-casted on the surface of the glassy carbon disk with a designated loading of 20 μg_{Pt} cm^{-2} and dried at room temperature to yield a uniform thin-film electrode. All the cyclic voltammetry (CV) and ORR polarization curves were recorded in 0.1 M $HClO_4$ (70 wt.%, double distilled, VERITAS, GFS Chemicals, Powell, OH, USA) and the ORR activity was measured in 0.1 M $HClO_4$ saturated with O_2 at 1600 rpm using linear sweep voltammetry (LSV) polarization plots at a scan rate of 10 mV s^{-1}.

MEA fabrication. MEA was prepared using the catalyst coated membrane (CCM) method where the catalyst ink was directly sprayed onto the proton exchange membrane (Gore® 10 μm) sitting on a hot plate at 70 °C. Active geometric area of MEA is 5 cm^2, 3.51 cm x 1.42 cm. For comparison, identical anode catalyst layers were prepared with Pt loading of 0.1 $mg_{Pt} \cdot cm^{-2}$ (±0.01) using 20wt.% Pt-XC72 (Jiping®, Shanghai, China) with 0.45 I/C ratio through same CCM method mentioned above. For the cathode, except for the catalyst difference, all conditions were the same including Pt loading, I/C ratio, and the solvents. The Pt loadings of cathode was controlled to 0.107 $mg_{Pt} \cdot cm^{-2}$ (±0.01) The MEA was assembled with Sigracet® 22BB gas diffusion layer (GDL) (SIG, Germany).

MEA testing protocols. Differential flow field cell (Figure S13) was applied for MEA testing. MEA was tested using fuel cell testing station (850e, Scribner Associate, Southern Pines, NC) at 80 °C, 100% RH, with flow rate of anodic (H_2) and cathodic (air) in 500 standard cubic centimeter per minute (sccm) and 2000 sccm, respectively under 150 kPa_{abs} for both sides. Testing protocols from the US Department of Energy (DOE) were used. MEA was tested by scanning voltage from 0.35 V to open circuit voltage (OCV) with 50 mV/step and holding 60s for each point, the corresponding current density was taken by averaging the values in last 15 seconds. Mass activity (MA) measurement follows the DOE protocol at 80 ° C and 100 % RH under pressure of 150 kPa_{abs}. The anodic flow (H_2) and cathodic flow (O_2) are 500 sccm and 2000 sccm, respectively. The MA was obtained by holding the cell voltage at 0.6 V for 5min, then, holding voltage at 0.9V $_{iR\text{-}Free}$ for 15 min and taking the average value of current in last 5 min, which was recorded every second.

Limiting Current testing protocol. Limiting current testing of a MEA was conducted in a differentia cell following the polarization curve test. The reactants are H_2 and the mixture of 2 vol.% of O_2 in N_2 for anode and cathode, respectively, with flow rates of 500/2000 sccm. The current density was first measured at 0.1 V, 0.15 V, 0.2 V and 0.3 V by holding at certain voltages for 2 min and record the average of current value in last 15 s. The limiting currents measured at 0.1 V were used for total O_2 diffusion resistance calculation. The limiting current density and R_{total} relationship is shown as in the Eq. S1, where F is Faraday constant, 96485 C/mol, x_O^{dry-in} is mole fraction of oxygen in dry mass, i_{lim} (A) is limiting current. The total O_2 diffusion resistance under different pressure was recorded and calculated. Then, the O_2 diffusion resistance was plotted against the pressure. The pressure independent resistance was obtained from the intercept of the plots[4]. In order to distinguish the gas phase O_2 diffusion resistance in catalyst layer $R_{CL,gas}$ and the O_2 diffusion resistance through the ionomer film, $R_{CL,ion}$, the limiting current density difference in relative humidifies (RHs) was measured.[5]

$$R_{total} = \frac{4Fx_O^{dry-in}p - p_w}{i_{lim} \quad RT} \qquad \text{Eq. S1}$$

For the limiting current measured in low relative humidity (RH), after polarization curve measured, the cathode gas was controlled to 20% RH, and MEA was purged under N_2 for both sides' electrode for 16 hours, then the limiting current density test followed the exact protocol as mentioned above.

O_2 diffusion resistance calculation. The O_2 diffusion resistance was calculated using the equation listed below.

$$R_{CL,ion} = \frac{\delta_{ion}^{eff} \; H_{ion,O_2}}{A_{ion}^{eff} D_{ion,O_2} RT} \quad \text{Eq. S2}$$

$$\Psi_{ion,O_2} = \frac{D_{ion,O_2}}{H_{ion,O_2}} = 3.27 \times 10^{-15} exp[1.28(RH)] \times \quad \text{Eq. S3}$$

$$R = 8.3145 \left(J \cdot mol^{-1} \cdot K^{-1} \right)$$

$$R_{total} = R_{DM} + R_{CL,gas} + R_{CL,ion} \quad \text{Eq. S4}$$

Since R_{DM} and $R_{CL,gas}$ are constant for a given electrode, then

$$R_{total}^{RH_1} - R_{total}^{RH_2} = R_{CL,ion}^{RH_1} - R_{CL,ion}^{RH_2} \quad \text{Eq. S5}$$

Eq. S3 could be reduced to $\Psi_{ion,O_2} = a \times exp[1.28(RH)]$ under given temperature. Where a is constant, defined in Eq. S6.

$$a = 3.27 \times 10^{-15} \times exp\left[\frac{17{,}200}{R}\left(\frac{1}{323.15} - \frac{1}{T}\right)\right] \left(mol \cdot \; s^{-1} \cdot m^{-1} \cdot Pa^{-1}\right) \quad \text{Eq. S6}$$

$$\Psi_{ion,O_2} = a \times exp[1.28(RH)] \quad \text{Eq. S7}$$

For all MEAs were tested under 353 K, thus, a is constant for these cases. Then, combining Eq. S2, Eq. S5 and Eq. S7, we have Eq. S8 as below.

$$R_{total}^{RH_1} - R_{total}^{RH_2} = R_{CL,ion}^{RH_1} - R_{CL,ion}^{RH_2} = \frac{q}{\Psi_{ion,O_2}^{RH_1} RT} - \frac{q}{\Psi_{ion,O_2}^{RH_2} RT} = \cdot \quad \text{Eq. S8}$$
$$q\left\{\frac{exp\left[-1.28\left(RH_1\right)\right] - exp\left[-1.28\left(RH_2\right)\right]}{RTa}\right\}$$

Reorganize the Eq. S8, then, q becomes Eq. S9

$$q = \left\{ \frac{R_{total}^{RH_1} - R_{total}^{RH_2}}{exp\left[-1.28(RH_1)\right] - exp\left[-1.28(RH_2)\right]} \right\} RTa \qquad \text{Eq. S9}$$

Given

$$b = \left\{ \frac{RTa}{exp\left[-1.28(RH_1)\right] - exp\left[-1.28(RH_2)\right]} \right\} \qquad \text{Eq. S10}$$

Where b is constant under the given temperature and the RH difference

Substitute Eq. S10 into Eq. S9, then, the Eq. S11 is obtained,

$$q = \left(R_{total}^{RH_1} - R_{total}^{RH_2}\right) b \qquad \text{Eq. S11}$$

Under a given temperature and ^{RH_1}and ^{RH_2}, e.g., 80% RH and 20% RH at 353 K, b is constant. Then q is proportional to the difference, $\left(R_{total}^{RH_1} - R_{total}^{RH_2}\right)$.

The q for three MEAs are named as $^{q_{NH_2}}$, q_{Blank} and $^{q_{SO_3H}}$. Here we use $^{q_{NH_2}}$ as baseline to calculate the ratio between $^{q_{NH_2}}$ and q_{Blank}, $^{q_{NH_2}}$ and $^{q_{SO_3H}}$:

$$\frac{q_{Blank}}{q_{NH_2}} = \frac{\delta_{ionBlank}^{eff}}{A_{ionBlank}^{eff}} \cdot \frac{A_{ionNH_2}^{eff}}{\delta_{ionNH_2}^{eff}} = \frac{\delta_{ionBlank}^{eff}}{\delta_{ionNH_2}^{eff}} \cdot \frac{A_{ionNH_2}^{eff}}{A_{ionBlank}^{eff}} \qquad \text{Eq. S12}$$

Here, A_{ion}^{eff} is proportional to Pt surface area $^{A_{Pt}}$which is related to ECSA of MEA[5].

$$\frac{q_{Blank}}{q_{NH_2}} \approx \frac{\delta_{ionBlank}^{eff} A_{PtNH_2}}{\delta_{ionNH_2}^{eff} A_{PtBlank}} \approx \frac{\delta_{ionBlank}^{eff} ECSA_{NH_2}}{\delta_{ionNH_2}^{eff} ECSA_{Blank}} \qquad \text{Eq. S13}$$

From Fig.6, ECSA of NH_2, Blank and SO_3H MEAs are 53.28, 46.42 and 25.31 m^2_{Pt}/mg_{Pt}, respectively. Then, substitute these values into Eq. S13 to obtain the following.

$$\frac{q_{Blank}}{q_{NH_2}} \approx \frac{\delta_{ionBlank}^{eff} ECSA_{NH_2}}{\delta_{ionNH_2}^{eff} ECSA_{Blank}} = \frac{\delta_{ionBlank}^{eff}}{\delta_{ionNH_2}^{eff}} \times 0.87 \qquad \text{Eq. S14}$$

$$\frac{q_{Blank}}{q_{NH_2}} = \frac{\left(R_{total}^{RH_1} - R_{total}^{RH_2}\right)_{Blank}}{\left(R_{total}^{RH_1} - R_{total}^{RH_2}\right)_{NH_2}} = \frac{0.05656}{0.02448} \qquad \text{Eq. S15}$$

Then:

$$\frac{q_{Blank}}{q_{NH_2}} = \frac{0.05656}{0.02448} \approx \frac{\delta^{eff}_{ionBlank}}{\delta^{eff}_{ionNH_2}} \times 0.87 \qquad \text{Eq. S16}$$

Finally, we have the ratios of effective thickness of ionomer films for both pairs as below.

$$\frac{\delta^{eff}_{ionBlank}}{\delta^{eff}_{ionNH_2}} \approx 2.66 \qquad \text{Eq. S17}$$

$$\frac{\delta^{eff}_{ionSO_3H}}{\delta^{eff}_{ionNH_2}} \approx 12.90 \qquad \text{Eq. S18}$$

(a)

(b)

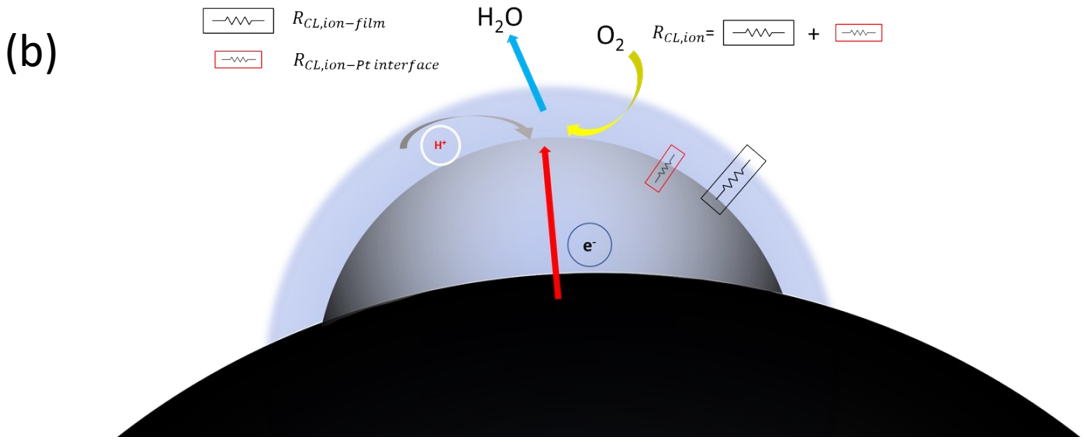

Figure. S1. Schematic of (a) catalyst ink drying process, (b) ionomer film and related O_2 diffusion resistances.

2. Additional results and discussion

Catalyst particle size distribution

TEM images of CLs from tested MEAs are shown Figure S2. The Pt NPs distribution was shown in Figure S2d. Although the average particle sizes of three Pt NPs are similar, there are few particles from SO_3H catalyst are larger than 6 nm in diameter, suggesting that there are still some large Pt NPs for SO_3H functionalized carbon supports, suggesting that the negatively charged carbon may not facilitate the uniform distribution of Pt NPs. But this small particle size difference is not sufficient to altering MEA performance in this work.

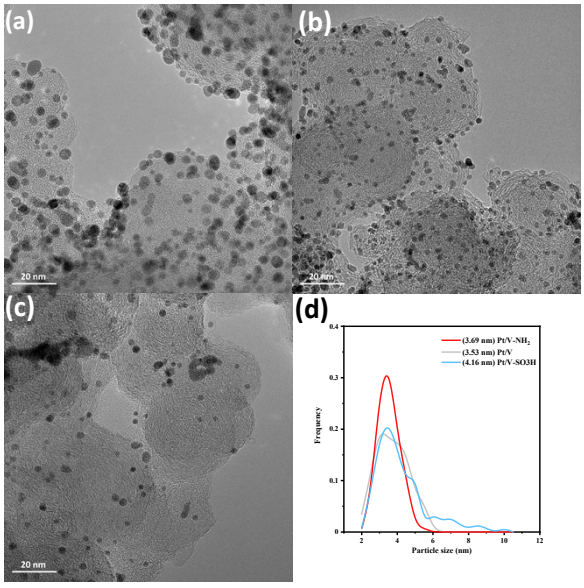

Figure. S2. Transmission electron microscope (TEM) imagines and Pt nanoparticles distributions of (a) Pt/V_{NH_2}, (b) Pt/V, and (c) Pt/V_{SO_3H} catalysts; (d) particles size distributions of Pt/V_{NH_2}, Pt/V and Pt/V_{SO_3H} catalysts (~150 counting)

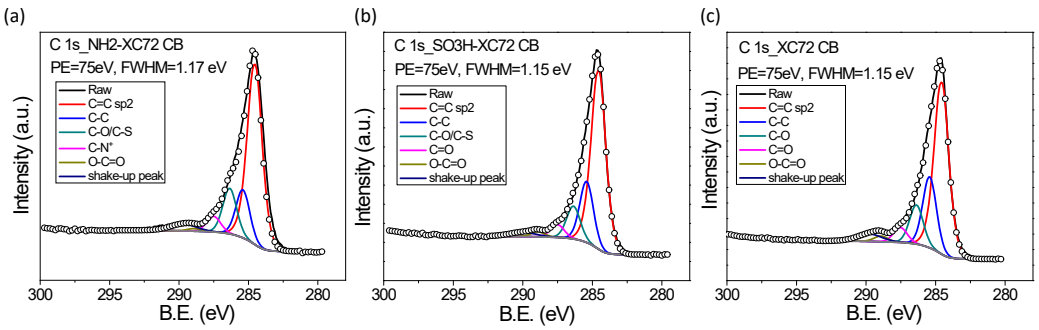

Figure. S3. XPS analysis for (a) Pt/V_{NH_2}, (b) Pt/V, and (c) Pt/V_{SO_3H} catalysts.

From the XPS results, we can extract the element composition in atomic percentage, see Supplementary table I. There are 1.3 at. % sulfur on XC72-SO_3H carbon, and 6.6 at.% nitrogen on XC72-NH_2 carbon, suggesting that SO_3H and NH_2 groups were successfully covalent-grafted on XC72-SO_3H and XC72-NH_2 carbons, respectively. However, no sulfur and nitrogen elements were detected on blank carbon.

Supplementary Table I. Summary of Figure. S3.

	Elemental composition (in atomic percentage)			
	C	O	S	N
Blank	90.0	10	N/A	N/A
SO3H-XC72	84.3	14.4	1.3	N/A
NH2-XC72	84.6	8.9	N/A	6.6

Besides, after functionalization, the surface energy of functionalized carbons regard to water is changed, from 87.44 mJ·cm^{-2} of Blank to 110.2 mJ·cm^{-2} and 230.5 mJ·cm^{-2} of NH_2 functionalized and SO_3H functionalized carbons, respectively (Supplementary table II). The surface energy of SO_3H is the largest among the three carbons, suggesting that SO_3H carbon is the most hydrophilic one. Assuming the same ionomer coverage among three types of CL, for a certain RH interval (e.g., 20% - 80% RH), the difference of O_2 diffusion resistance of SO_3H CL should have been the smallest because the high hydrophilicity should result in small O_2 diffusion resistance at low RH than others. However, the reality is opposite, the MEA performance at the same RH interval did not show such a trend. This contradiction suggests that the electrostatic force here, plays a more dominant role in controlling the ionomer and catalyst interaction than the surface energy does.

Supplementary Table II. Summary of surface energy of three carbons.

	Nitrogen sorption		Water sorption	
	Surface Area (m^2/g)	Spreading Pressure	Liquid-Solid Work of Adhesion	Total Surface Energy (mJ/m^2)

		(mJ/m^2)	(mJ/m^2)	
Blank	254.0	14.6	158.7	87.4
SO_3H-XC72	110.4	109.7	253.7	230.5
NH_2-XC72	93.6	36.5	180.6	110.2

ITC raw data and fitted data.

To calculate entropic and enthalpic contributions to binding, it is necessary to use a molar basis. Molar concentrations are calculated following the procedure as previously reported[1]. As the molecular weight or the polydispersity of the ionomer are not precisely known, the monomer molar concentration is calculated from the mass concentration and equivalent weight. For example, 3.25 mg/mL of 720 EW Aquivion is calculated to be 4.514 mM. The mole of catalyst binding sites is calculated using, the surface area of particles—based on density of Vulcan XC72 (264 kg/m^3) and primary particle size (50 nm diameter)—and the projected area of ionomer aggregate (assuming a 3 nm x 10 nm cylinder)[6]. For 0.5 mg/mL XC72, the concentration is calculated to be 0.054 mM. Thermodynamic parameters are extracted from the binding model using this molar basis. Specifically, the extracted binding constant is related to the free energy by ($|\Delta G| = RT\ln[KA]$). Using the enthalpic contribution from the isotherm, entropic contributions are calculated using $\Delta G = \Delta H - T\Delta S$.

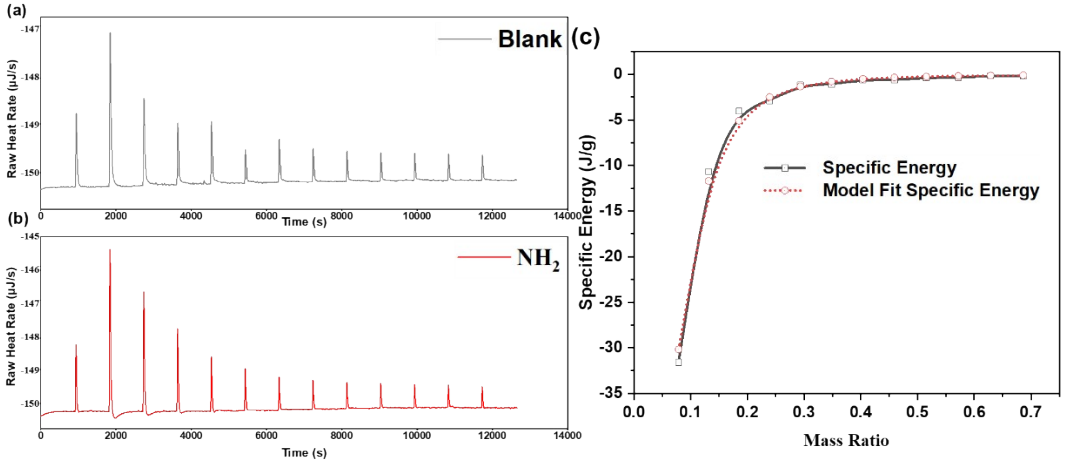

Figure. S4. Example raw data of (a) blank, (b) XC72-NH_2 and binding curve (c).

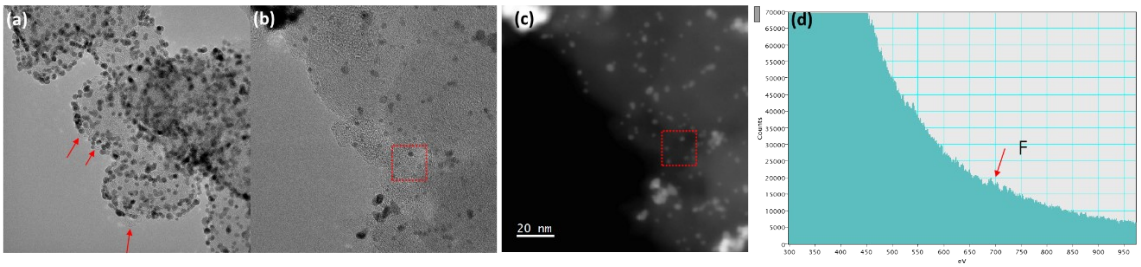

Figure. S5. (a) Pt/V catalyst BF-TEM image without ionomer, (b) SO_3H BF-TEM with ionomer, and (c-d) STEM-EELS of same area as figure 4i.

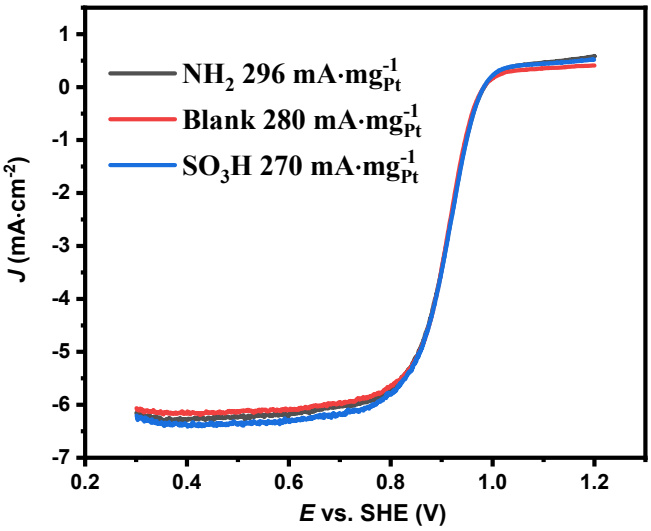

Figure. S6. Steady-state ORR polarization plots of Pt/V-NH, Pt/V and Pt/V-SO_3H catalysts in 0.1 M $HClO_4$.

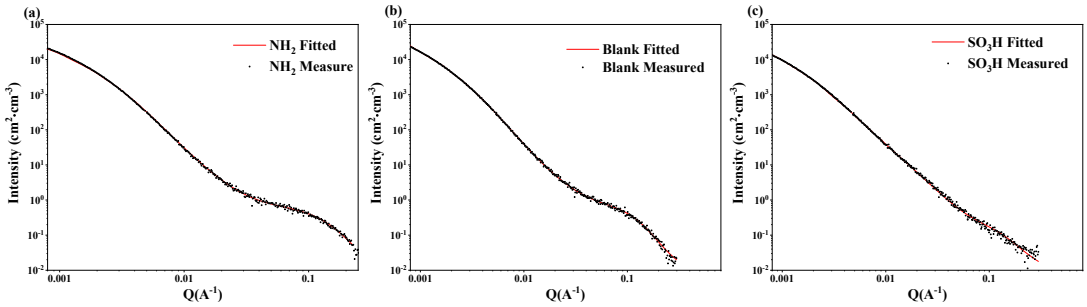

Figure. S7. Raw and fitted USAXS data of three catalysts' ink.

MEA performance in Helox and different RH

The Helox (21 vol% O_2 in He) test of three MEA is performed with same testing protocol as the air performance of MEA. The performance comparison is shown in Figure S7.

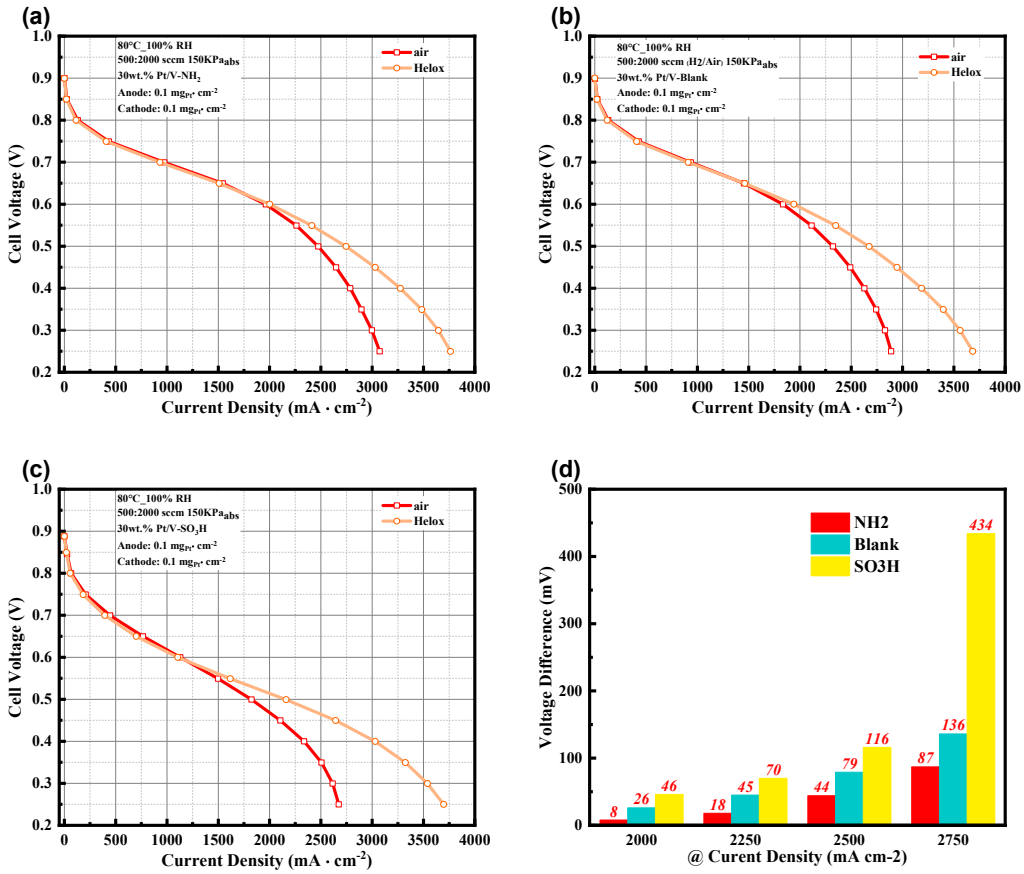

Figure. S8. Performance comparison in Helox and air testing of (a) NH_2 catalyst, (b) Blank catalyst, and (c) SO_3H catalyst. (d) Summary of performance gained in helox test of three MEAs.

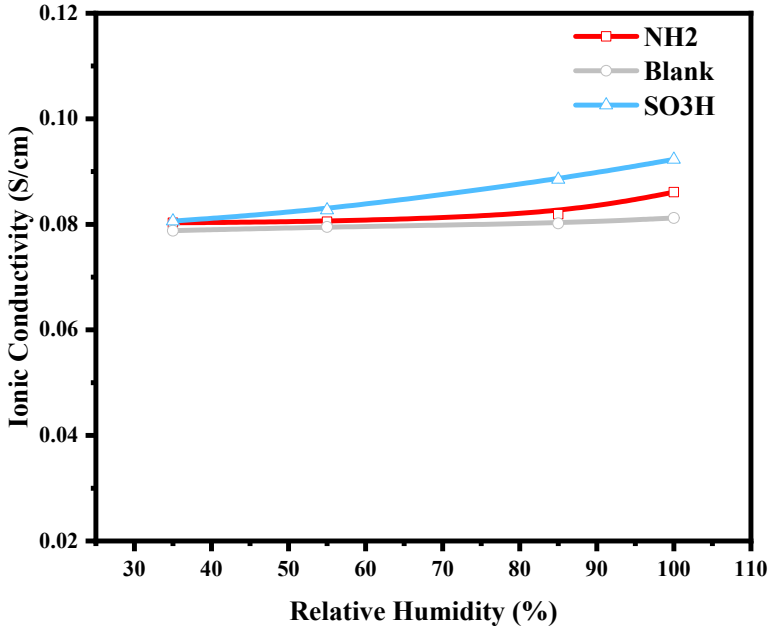

Figure. S9. Ionic conductivity of three catalysts against RH.

The performance of three MEAs in different RHs is shown in Figure S7. NH_2 MEA performance is monotonically increasing with RH, and so does the blank MEA. However, for the SO_3H MEA, the performance is monotonically increasing with RH except for RH above 80 %. SO_3H MEA performance at 100 % RH is lower than that at 80%. It is due to the high surface energy of SO_3H catalyst so that under saturate condition, in high current density range (e.g., > 2 A cm^{-2}), water flooding happens. Under these circumstances, the use of limit current density data at 80 % RH for calculating O_2 diffusion resistance is more reliable.

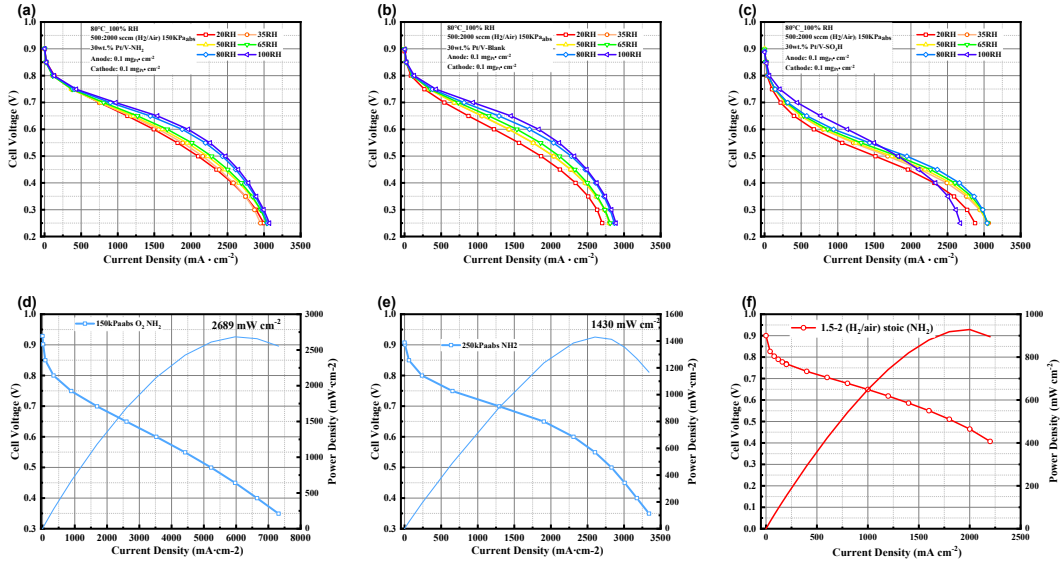

Figure. S10. MEA performance under 20%, 35%, 50%, 65%, 80%, and 100 % RH of (a) Pt/V_{NH2}, (b) Pt/V, (c) Pt/V_{SO3H} catalysts (0.1mg_{Pt} cm^{-2}) (H_2-air fuel cell I-V polarization curves recorded under 150 kPa_{abs} of air pressure); (d) Pt/V_{NH2} (H_2-air fuel cell I-V polarization curve recorded under 250 kPa_{abs} of air pressure); (e) MEA performance under 100 % RH of the Pt/V_{NH2} , H_2-O_2 fuel cell I-V polarization curve recorded under 150 kPa_{abs}; (f) MEA performance of Pt/V_{NH2} with 1.5/2 stoic for H_2/air, the geometric of MEA is 25 cm^2.

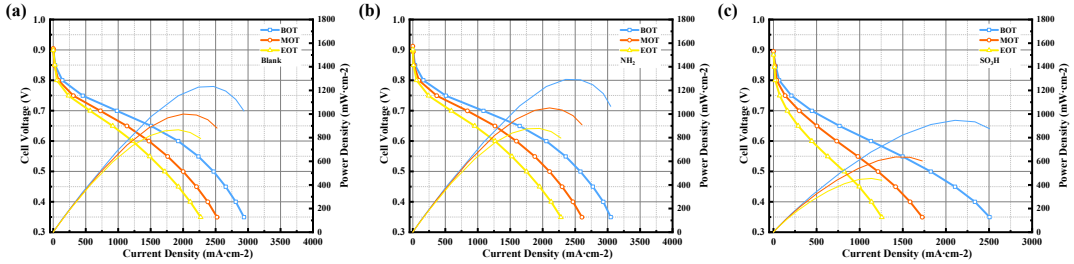

Figure. S11. H2/air fuel cell BOT and EOT polarization curves for MEA coated (a) Pt/V-NH_2 and (b) Pt/V, and (c) Pt/V-SO_3H. All MEAs with 0.1 mg_{Pt} cm^{-2} loading in both the cathode and anode and were measured under 100% relative humidity at 80 °C with 150 $kPa_{abs.}$

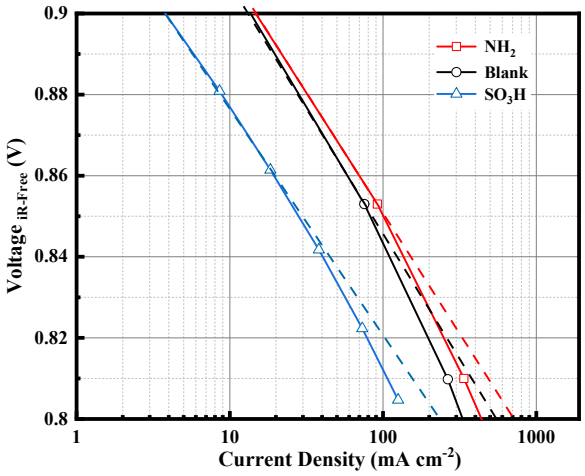

Figure. S12, Tafel plot of three MEAs. (80 °C 150 kPa_{abs} pressure with 200/400 sccm H_2/O_2)

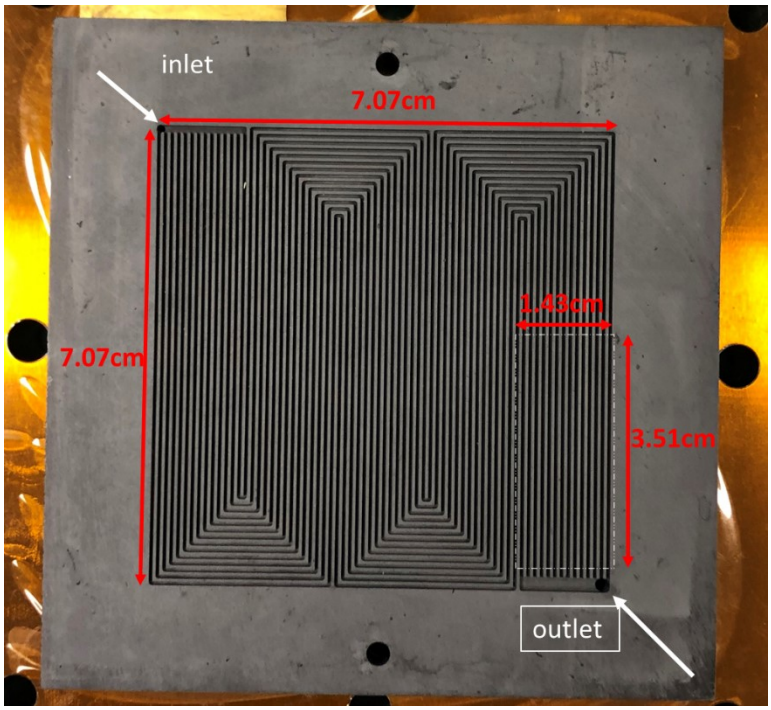

Figure. S13. Differential flow field is used in this work with detailed flow channels. 5 cm^2 MEA was placed in the white dash box. The differential cell design follows Baker, Daniel R et al. work[4].

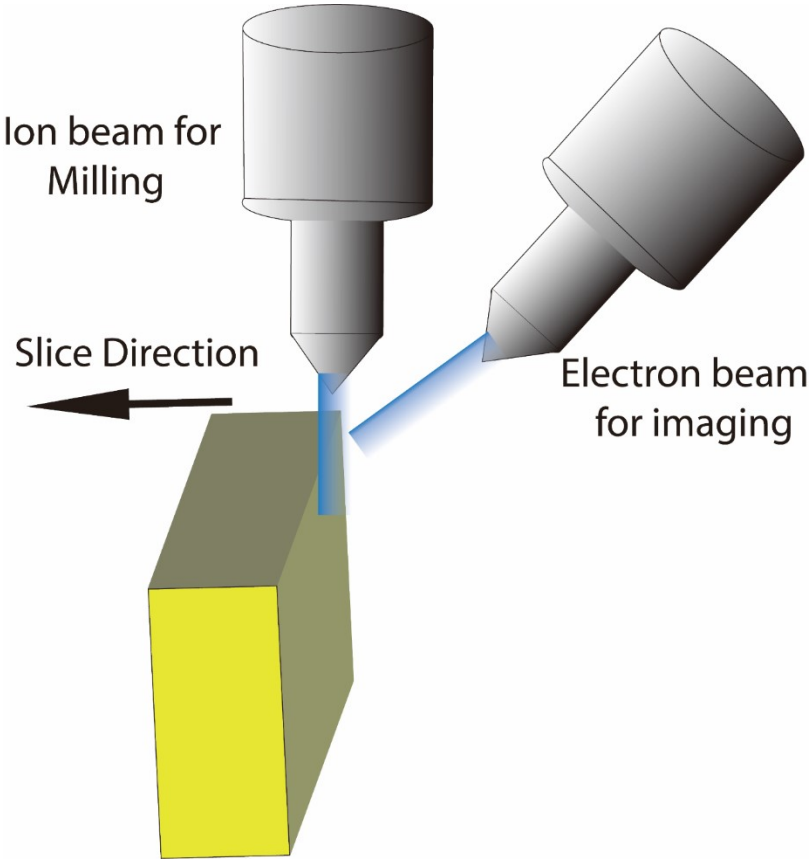

Figure. S14 Schematic of FIB-SEM set up.

Supplementary Table III. MEA Performance comparison of major published work
Supplementary Table III. MEA Performance comparison of major published work

Catalyst	Cathode loading (mg_{Pt} cm^{-2})	Peak power density (mw cm^{-2})	Rated power density (mw cm^{-2})	Flow rate (a/c) (sccm)	Membrane	Absolute operating pressure (kPa)	Ref
PtNi-BNCs	0.15	920(H_2-air)	802(H_2-air)	150/300	NF212 50 μm	306.8 (256.8 partial pressure of air)	Science 2019, 366, 850–856.[7]
LP@PF-2	0.0035-0.0043	1450(H_2-O_2) 1050(H_2-air)	N/A 670(H_2-air)	200/520	NF211 25 μm	200 (150 partial pressure of air/O_2)	Science 2018, 362, 1276-1281.[8]
PtA@FeSA-N-C	0.13	1310(H_2-O_2)	N/A	N/A	NF211 25 μm	150 (100 partial pressure of air)	Energy Environ. Sci. 2020, 13, 3032-3040.[9]
Pt/N-KB 600 °C	0.10	1390(H_2-air)	871(H_2-air)	500/2000	Gore MX20.10 (10 μm)	230 (170 partial pressure of air)	Nat. Mater. 2020, 19, 77-85.[10]
PtNiN/KB	0.10	N/A	837(H_2-air)	500/2000	NF211 25μm	150 (100 partial pressure of air)	ACS Catal. 2020, 10, 10637−10645.[11]
L10-PtZn/Pt-C	0.14	2000(H_2-O_2) 960(H_2-air)	N/A 716(H_2-air)	500/1000 500/1000	NF211 25 μm	150 (100 partial pressure of air) 150 (100 partial pressure of air)	Adv. Energy. Mater. 2020, 10, 2000179[12]
PtNi-N1	0.40	~900 (H_2-air)	730 (H_2-air)	Stoic flow Stoic ratio (1.5/2)	NF211 25 μm	170 (120 partial pressure of air)	Energy & Environmental Science **8**, 258-266[13]
Pt1Co1-IMC@Pt/C	0.20	1230 (H_2-air)	740 (H_2-air)	400/1500	Gore MX20.10 (10 μm)	200 (150 partial pressure of air)	Energy & Environmental Science **15**, 278-286[14]
Pt/C	0.23	600 (H_2-air)	420 (H_2-air)	Stoic flow Stoic ratio (1.5/1.8)	Gore MX (18 μm)	250 (200 partial pressure of air)	Science 2021, 374, 459-464[15]
Pt/C	0.12	~800 (H_2-air)	502 (H_2-air)	300/500	NF211 25 μm	250 (200 partial pressure of air)	Nat. Catal. 2023[16]
Pt/V-NH2	~0.10	1237(H_2/air)	891(H_2/air)	500/2000 (Differential)	Gore MX20.10 (10 μm)	150 (100 partial pressure of air)	This work
		1430(H_2/air)	1150(H_2/air)	500/2000 (Differential)		250 (200 partial pressure of air)	
		900(H_2/air)	550 (H_2/air)	Stoic flow Stoic ratio (1.5/2)		150 (100 partial pressure of air)	

Supplementary Table IV. Summary of Figure S9.

Pt/V_{NH2}	BOL	EOL	Loss
MA ($mA \cdot mg_{Pt}^{-1}$)	188	120	68(36%)
E @ 0.8 A cm^{-2} (V)	724	670	54
J @ 0.67 V ($mA\ cm^{-2}$)	1416	807	609

Pt/V	BOL	EOL	Loss
MA ($mA \cdot mg_{Pt}^{-1}$)	164	107	57(42%)
E @ 0.8 A cm^{-2} (V)	716	666	50
J @ 0.67 V ($mA\ cm^{-2}$)	1292	773	519

Pt/V_{SO3}	BOL	EOL	Loss
MA ($mA \cdot mg_{Pt}^{-1}$)	78	54	24(30%)
E @ 0.8 A cm^{-2} (V)	644	506	138
J @ 0.67 V ($mA\ cm^{-2}$)	628	234	394

Supplementary Table V. Comprehensive summary of MEA specific activity (SA) at 0.9 V, 0.85 V, and 0.8V.

Catalyst	SA at 0.9 $V_{iR\text{-}free}$ ($mA\ cm^{-2}$)	SA at 0.85 $V_{iR\text{-}free}$ ($mA\ cm^{-2}$)	SA at 0.8 $V_{iR\text{-}free}$ ($mA\ cm^{-2}$)
Blank	0.345	1.745	7.066
NH2	0.357	1.896	8.164
SO3H	0.347	1.383	6.164

Reference

1. S. A. Berlinger, B. D. McCloskey and A. Z. Weber, *Acs Energy Letters*, 2021, **6**, 2275-2282.
2. C. M. Popescu, C. A. S. Hill, R. Anthony, G. Ormondroyd and S. Curling, *Polymer Degradation and Stability*, 2015, **111**, 263-268.
3. D. Charriere and P. Behra, *J Colloid Interface Sci*, 2010, **344**, 460-467.
4. D. R. Baker, D. A. Caulk, K. C. Neyerlin and M. W. Murphy, *Journal of The Electrochemical Society*, 2009, **156**.
5. N. Nonoyama, S. Okazaki, A. Z. Weber, Y. Ikogi and T. Yoshida, *Journal of the Electrochemical Society*, 2011, **158**, B416-B423.
6. G. Gebel and J. Lambard, *Macromolecules*, 1997, **30**, 7914-7920.
7. X. Tian, X. Zhao, Y. Q. Su, L. Wang, H. Wang, D. Dang, B. Chi, H. Liu, E. J. M. Hensen, X. W. D. Lou and B. Y. Xia, *Science*, 2019, **366**, 850-856.
8. L. Chong, J. Wen, J. Kubal, F. G. Sen, J. Zou, J. Greeley, M. Chan, H. Barkholtz, W. Ding and D. J. Liu, *Science*, 2018, **362**, 1276-1281.
9. X. Ao, W. Zhang, B. T. Zhao, Y. Ding, G. Nam, L. Soule, A. Abdelhafiz, C. D. Wang and M. L. Liu, *Energy & Environmental Science*, 2020, **13**, 3032-3040.
10. S. Ott, A. Orfanidi, H. Schmies, B. Anke, H. N. Nong, J. Hubner, U. Gernert, M. Gliech, M. Lerch and P. Strasser, *Nat Mater*, 2020, **19**, 77-85.
11. X. R. Zhao, C. Xi, R. Zhang, L. Song, C. Y. Wang, J. S. Spendelow, A. I. Frenkel, J. Yang, H. L. Xin and K. Sasaki, *Acs Catalysis*, 2020, **10**, 10637-10645.
12. J. Liang, Z. Zhao, N. Li, X. Wang, S. Li, X. Liu, T. Wang, G. Lu, D. Wang and B. J. Hwang, *Advanced Energy Materials*, 2020, **10**, 2000179.
13. B. H. Han, C. E. Carlton, A. Kongkanand, R. S. Kukreja, B. R. Theobald, L. Gan, R. O'Malley, P. Strasser, F. T. Wagner and Y. Shao-Horn, *Energy & Environmental Science*, 2015, **8**, 258-266.
14. Q. Cheng, S. Yang, C. Fu, L. Zou, Z. Zou, Z. Jiang, J. Zhang and H. Yang, *Energy & Environmental Science*, 2022, **15**, 278-286.
15. C.-L. Yang, L.-N. Wang, P. Yin, J. Liu, M.-X. Chen, Q.-Q. Yan, Z.-S. Wang, S.-L. Xu, S.-Q. Chu, C. Cui, H. Ju, J. Zhu, Y. Lin, J. Shui and H.-W. Liang, *Science*, 2021, **374**, 459-464.
16. F. Chen, S. Chen, A. Wang, M. Wang, L. Guo and Z. Wei, *Nature Catalysis*, 2023, DOI: 10.1038/s41929-023-00949-w.